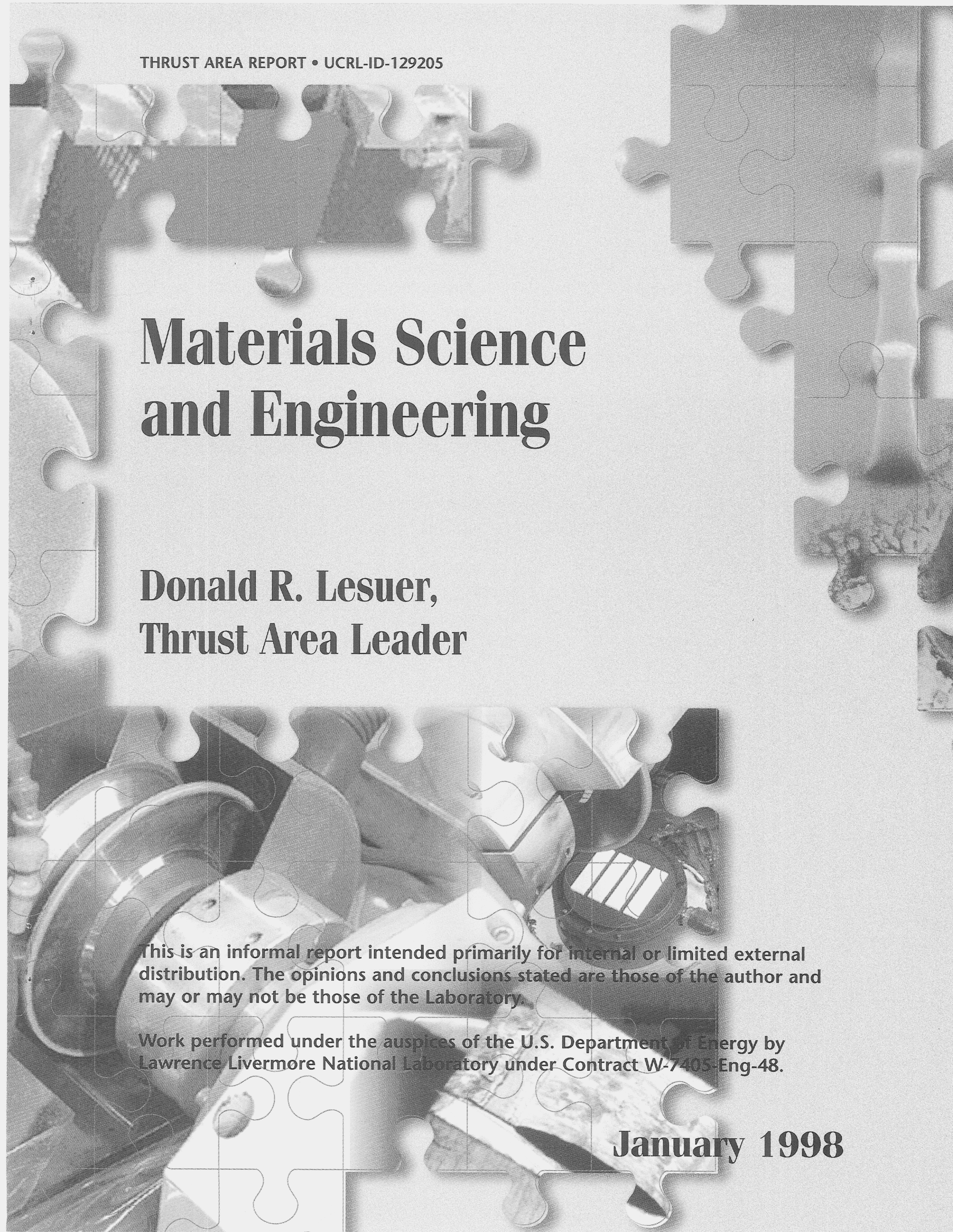

THRUST AREA REPORT • UCRL-ID-129205

# Materials Science and Engineering

## Donald R. Lesuer,
## Thrust Area Leader

This is an informal report intended primarily for internal or limited external distribution. The opinions and conclusions stated are those of the author and may or may not be those of the Laboratory.

Work performed under the auspices of the U.S. Department of Energy by Lawrence Livermore National Laboratory under Contract W-7405-Eng-48.

**January 1998**

Disclaimer

This document was prepared as an account of work sponsored by an agency of the United States Government. Neither the United States Government nor the University of California nor any of their employees, makes any warranty, express or implied, or assumes any legal liability or responsibility for the accuracy, completeness, or usefulness of any information, apparatus, product, or process disclosed, or represents that its use would not infringe privately owned rights. Reference herein to any specific commercial products, process, or service by trade name, trademark, manufacturer, or otherwise does not necessarily constitute or imply its endorsement, recommendation, or favoring by the United States Government or the University of California. The views and opinions of authors expressed herein do not necessarily state or reflect those of the United States Government or the University of California, and shall not be used for advertising or product endorsement purposes.

This report has been reproduced
directly from the best available copy.

Available to DOE and DOE contractors from the
Office of Scientific and Technical Information
P.O. Box 62, Oak Ridge, TN 37831
Prices available from (615) 576-8401, FTS 626-8401

Available to the public from the
National Technical Information Service
U.S. Department of Commerce
5285 Port Royal Rd.,
Springfield, VA 22161

THRUST AREA REPORT • UCRL-ID-129205

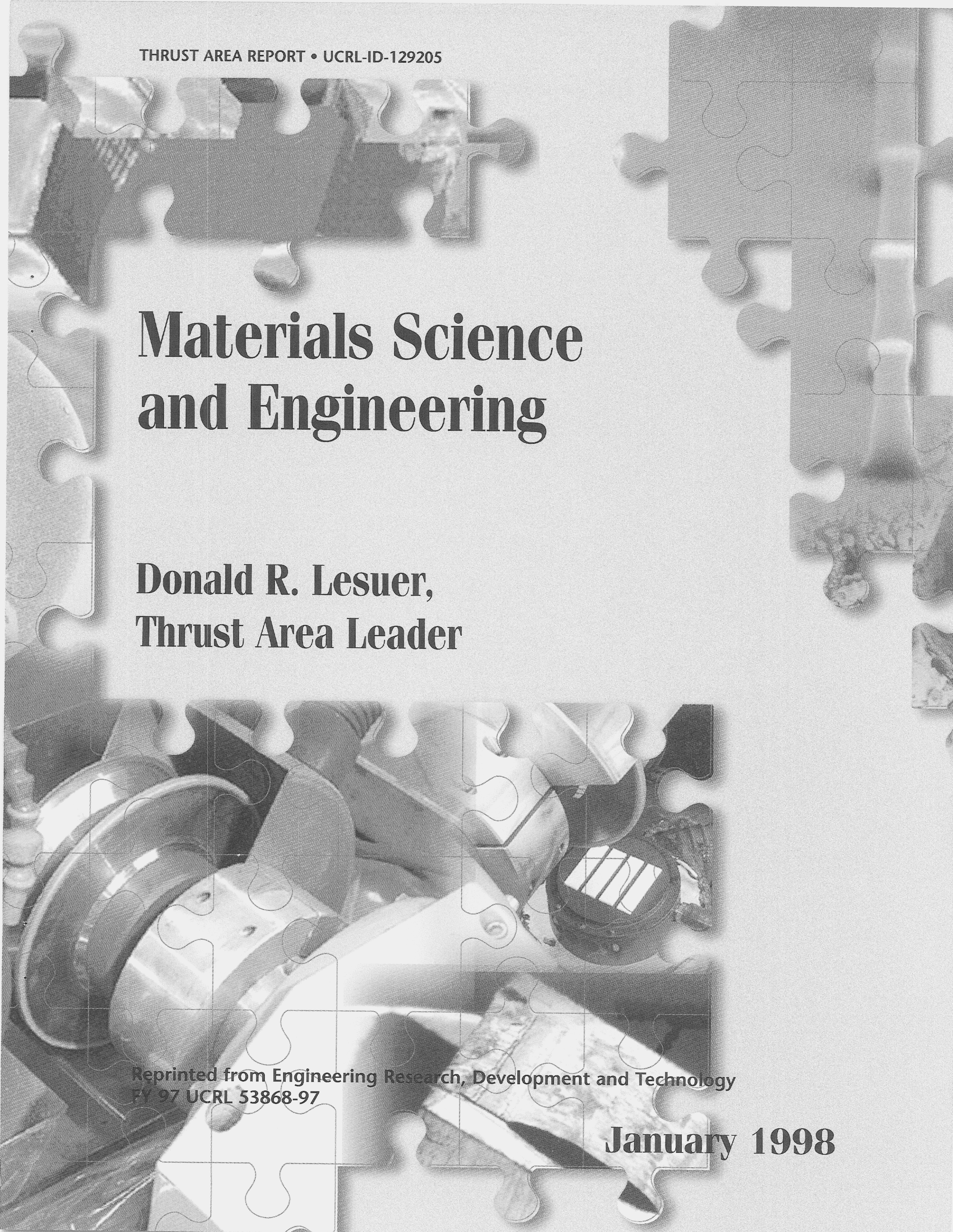

# Materials Science and Engineering

## Donald R. Lesuer, Thrust Area Leader

Reprinted from Engineering Research, Development and Technology
FY 97 UCRL 53868-97

January 1998

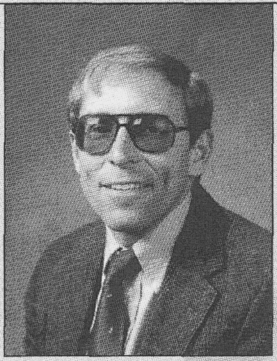

## Donald R. Lesuer, Thrust Area Leader

During FY-97, work within the Materials Science and Engineering thrust area was focused on material modeling. Our motivation for this work is to develop the capability to study the structural response of materials as well as materials processing.

These capabilities have been applied to a broad range of problems, which support many programs at Lawrence Livermore National Laboratory. Recent examples of structural response problems studied include material fracture (such as interface failure), damage in laser optics, the response of weapons components (such as high explosives) and the failure of composite materials. For materials processing, typical problems studied include metal forming, laser processing, casting, and heat treating.

To improve our ability to model material behavior, much of our work involves developing new material models and failure models, as well as applying the codes to new problems. Most investigations involve experimental studies to gather basic information on material response and to validate codes or material models. Projects are inherently multi-disciplinary, involving several investigators with expertise in materials and mechanics.

Our thrust area studies for FY-97 are described in the following three articles: 1) Evolution of Anisotropic Yield Behavior; 2) Modeling of She Localization in Materials; and 3) Modeling of Casting Microstructures and Defect

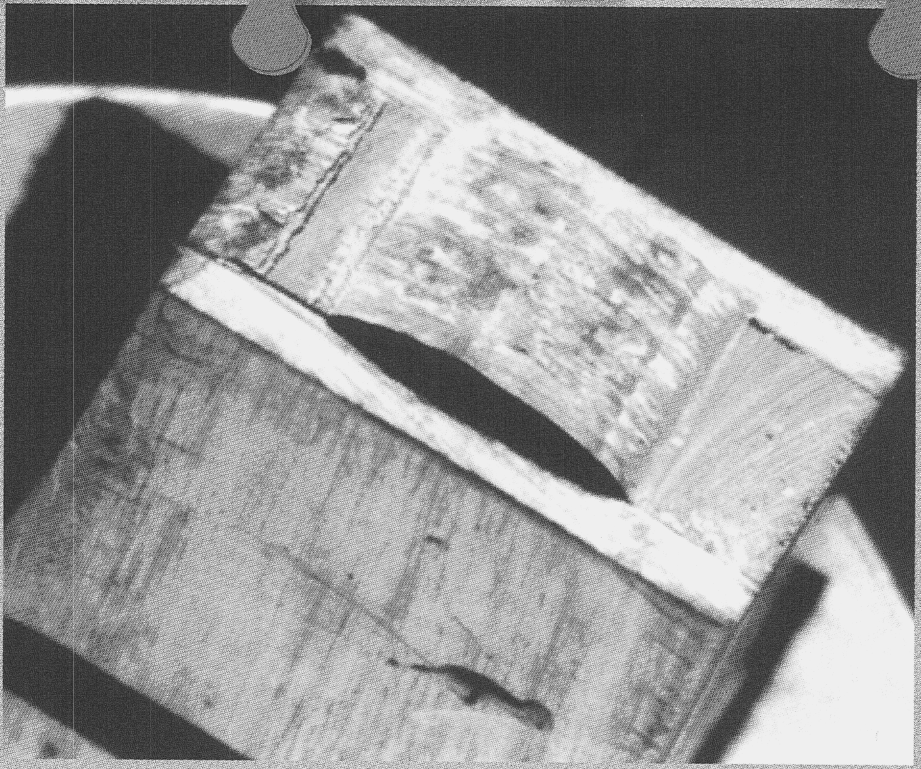

# Materials Science and Engineering

# 5

# 5. Materials Science and Engineering

**Overview**
*Donald R. Lesuer, Thrust Area Leader*

**Evolution of Anisotropic Yield Behavior**
*Daniel J. Nikkel, Jr., Arthur A. Brown, and James Casey ....................5-1*

**Modeling of Shear Localization in Materials**
*Donald R. Lesuer, Mary M. LeBlanc, Robert A. Riddle, and Bert R. Jorgensen....................5-7*

**Modeling of Casting Microstructures and Defects**
*Arthur B. Shapiro and J. Del Eckels ....................5-13*

# Evolution of Anisotropic Yield Behavior

**Daniel J. Nikkel, Jr.**
*Manufacturing and Materials Engineering Division*
*Mechanical Engineering*

**Arthur A. Brown and James Casey**
*University of California*
*Berkeley, California*

We have developed an experimental capability for measuring the yield behavior of elastic-plastic materials under multiaxial loading conditions. This enables us to determine the multi-dimensional yield surface of the material, both in its initial state and as it evolves during large inelastic deformations. This surface, and its functional representation, is an essential component of the constitutive theory for non-linear anisotropic elastic-plastic materials. Experimental data provided by this facility aids the development of more physically realistic and complete models for materials undergoing large inelastic deformations.

## Introduction

Generally speaking, polycrystalline metals subjected to loads or deformations initially exhibit elastic (reversible) behavior. However, if the deformation or loads become large enough, the material begins to exhibit plastic behavior (that is, there is no longer a one-to-one correspondence between stress and strain, the stress response is path dependent, and residual—plastic—deformations remain after external loads are removed.) This gives rise to the theoretical idealization of an elastic-plastic material, and in particular, the notion of a yield function,[1]

$$f\left(s_{kl}, e^{p}_{kl}, k, \ldots\right) = g\left(e_{kl}, e^{p}_{kl}, k, \ldots\right) \quad .$$

This relationship, a key ingredient of the constitutive theory of elastic-plastic materials, describes the boundary between loads (or deformations) that produce only elastic behavior, and those that result in inelastic deformation (**Fig. 1**). Here, $s_{kl}$ denotes the components of the stress tensor; $e_{kl}$ denotes the components of the strain tensor; $e^{p}_{kl}$ denotes the components of the plastic strain tensor; $k$ is a scalar measure of work hardening; and the ellipses represent other inelastic state variables that may be present, depending on the constitutive theory.

For fixed values of the inelastic variables, the yield condition described by $f = 0$ (or $g = 0$) can be interpreted geometrically from the point of view of stress space (or strain space), the multi-dimensional space whose axes are the components of stress (or strain), as a surface that bounds the region in which only elastic behavior occurs (the elastic region). As long as the loading of the material is such that the current state is enclosed by the yield surface, the material responds elastically. But if the loading causes the current state to intersect the yield surface and try to move outward from this surface, inelastic behavior occurs and plastic deformation results. The current state never moves outside the yield surface, but instead the surface is pushed along with it, and may also change shape as the inelastic deformation increases.

Most plasticity models implemented into numerical codes assume a fixed shape of the yield surface (for example, elliptical). What distinguishes different models is how the yield surface evolves, for example by allowing it to rigidly translate or to change in size while maintaining its shape according to some strain- (or strain-rate- or temperature-) dependent hardening law. While the initial yield surface of isotropic materials may be reasonably represented by an ellipse, subsequent to even moderate plastic deformation, the shape of the yield surface in real materials can change significantly **(Fig. 1)**. For this reason, simple representations of the yield function will be satisfactory only under very restrictive loading conditions (for example, monotonic or uniaxial), and are totally inadequate for general multiaxial loading conditions, during which loads can reverse and change direction during the history of loading.

Motivated by these considerations, and the fact that the vast majority of experimental data available is for uniaxial (and generally monotonic) loading, we have developed an experimental capability to map out the yield surface at various fixed states of large inelastic deformation under multiaxial states of loading. By determining the yield surfaces on a single specimen at multiple fixed states, the evolution of the yield surface during plastic deformation can be observed, and better quantitative representations of the yield function and hardening characteristics of the material can be developed. This will lead to better constitutive equations for anisotropic materials undergoing large inelastic deformations.

## Progress

The experimental determination of the yield surface of the material under two-dimensional loading is carried out by loading a specimen under multiaxial conditions and probing until the point of yield is reached, then backing off and probing in a different direction in stress space, until the entire surface is mapped out. A multiaxial MTS hydraulic test machine with an axial load capacity of ±50,000 lbf and ± 20,000 in.-lbf in torsion is used for these experiments.

Although it can operate in either load, strain, or displacement control modes, it was found best to carry out all testing in load control. For the small load and strain increments being used during yield surface probing, it was found that this method gave the best level of accuracy.

Preliminary tests showed that the ratio of load noise to load increment was significantly smaller than the ratio of strain noise to strain increment, and further, that displacement control was impossible, since the rotation increment corresponding to the desired rotation step size was more than a factor of 100 smaller than the noise in the rotation measurements.

There are three basic issues to be addressed in the development of this experimental capability: 1) specimen design and preparation; 2) automated control of the testing machine; and 3) experimental methodology for the determination of yield.

### Specimen Design

A specimen to be used for mechanical behavior characterization should have a gage section where the state of stress and deformation during testing are homogeneous, as are the material properties. For axial and torsional loading, this suggests using a thin-walled tubular specimen. To map out the entire yield surface (in the two-dimensional axial-torsional sub-space of stress-space), it is necessary to subject the specimen to positive and negative torsional loads in combination with tensile and compressive axial loads.

Moreover, one must be able to apply a large enough stress to cause significant plastic deformation (up to 20%) for the full range of experiments under consideration. A thin specimen can be susceptible

*Figure 1. Initial yield surface, and measured points on two subsequent yield surfaces, for a single 1100 aluminum specimen. The subsequent yield surfaces for pre-loads to point A, and then to B, show significant deviation from an idealized ellipse, even though the strains involved are moderately small.*

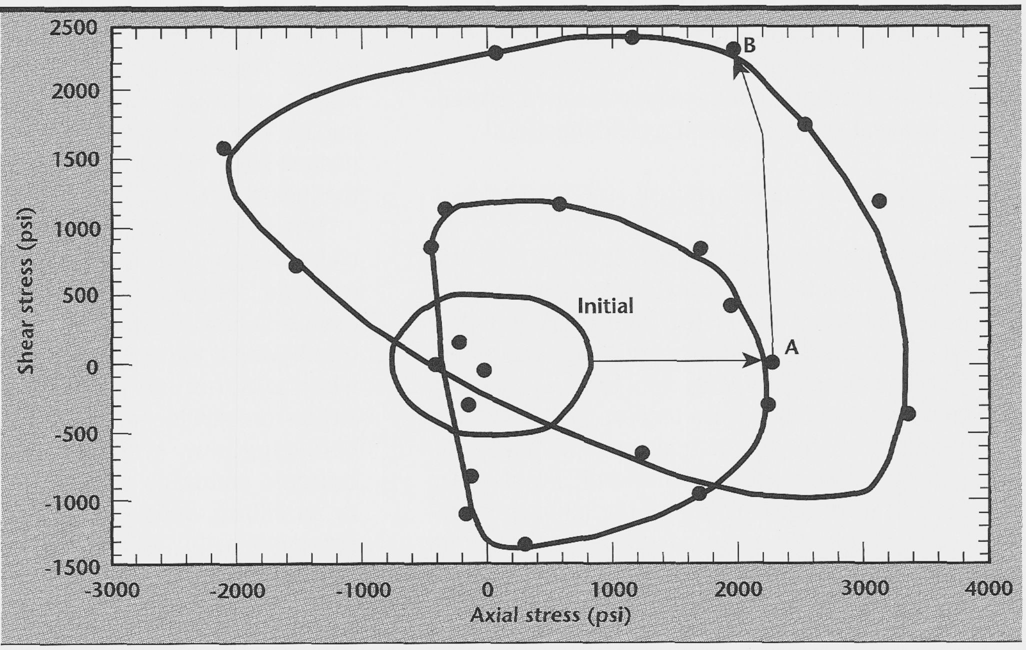

to buckling, and while making the specimen thicker makes it more resistant to buckling, this reduces the overall stress that can be applied to the material and compromises the homogeneity of the stress and strain state in the gage section during torsion.

In addition, it is desirable to make the overall specimen geometry compatible with other experiments making use of the machine so as to avoid redesign of fixturing.[2] Balancing these contrasting goals, a specimen geometry was arrived at, consisting of a circular cylinder 9 in. long (4 in. gage length), 2 in. inside diameter, with a 0.1-in. wall thickness. These specimens were machined out of thicker walled stock of 1100 aluminum, and the ends were potted with conical sections of epoxy to allow for gripping.

For the mechanical properties in the gage section to be sufficiently homogeneous, the microstructure of the specimen must be much finer than the wall thickness. This was accomplished through heat treatment. The first heat treatment tried, following Bell,[3] whose experiments we wished to compare ours with, resulted in extremely large grains that were unacceptable. The heat treatment process that was found to give the best grain structure followed Phillips[4]: heating to 650 °F in 15 min, and maintaining for 1 h, followed by furnace cooling. This resulted in equiaxed grains with an average size of 0.003 in.

## Test Machine Control and Data Acquisition

The numerical control of the test machine and the data acquisition are coordinated via a custom application written in LabView II for this project. This program communicates with the test machine's load cells and receives input from four strain gages affixed to the specimen. Three of the strain gages are in a 45° rosette, bonded in the center of the gage length such that the center gage element is in the longitudinal direction, and the other two elements are aligned at 45° to each side of the longitudinal axis.

One extra axial strain gage is placed diametrically opposite to the rosette and is used to check that the specimen is properly aligned and that no bending occurs during testing. The data inputs to the LabView program are the test machine's axial force, axial stroke, torsional load, and rotation, along with conditioned signals from the strain gages. The operator can specify end states (either as loads or displacements), as well as ramp rates of force and torque (or stroke and rotation) for getting from one fixed state to the next. Up to four different sets of cross-plotted output data are simultaneously presented, to visually observe the nature of the material behavior (**Fig. 2**).

## Experimental Methodology for Determination of Yield

The surface that we are trying to map is the yield surface at an arbitrary fixed inelastic state. Ideally, all points on a given yield surface should be determined without inducing any further plastic deformation to the specimen. In practice, however, a point on the yield surface can only be determined by reaching, and slightly exceeding, the yield point.

The challenge therefore, in developing an experimental procedure for mapping the surface, is to do it in such a way that all the points necessary to characterize a given surface (probably a minimum of 10 points) can be located while changing the inelastic state (and hence the surface itself) as little as possible. The procedure that has been developed can detect yield without producing a plastic strain greater than $5 \times 10^{-6}$, with a good level of repeatability.

From whatever load state the specimen is currently in, a linear load path segment in stress-space is specified, and is carried out in step increments in which no component of stress changes by more than 50 psi. Under multiaxial loading conditions, to see yielding occur, it is necessary to watch multiple components of the response simultaneously.

Observing the raw stress/strain response for different directions is not sufficiently sensitive to determine yield as soon as is desired. Instead, prior to reaching the yield surface, data is taken during purely elastic behavior, then the path is retraced. A best linear fit to the stress/strain response is determined, and a new modified strain measure for each component direction of interest is defined as the actual strain minus the fitted linear elastic response.

When the load vs modified strain output is observed during the test, the point at which yielding begins to occur is much clearer (**Fig. 2**). Prior to reaching the proportional limit, the data points are on a nearly vertical line. When three successive data points (with 1-microstrain error bars) fall away from the abscissa in three out of the four load vs modified strain plots (corresponding to different strain-gage directions), the specimen is considered to have yielded, and a point on the yield surface is identified. The load is then reversed, taking the specimen back to a state within the yield surface, and a new end state is sought.

This process is repeated until a sufficient number of points have been located on the yield surface to characterize it. Once the yield surface for one inelastic state is so obtained, an excursion involving plastic deformation can be applied to the same specimen, and the process described above can be repeated to map the yield surface for the new inelastic state.

**Figure 1** shows actual measured data from a single 1100 aluminum specimen, where the initial yield surface is shown, along with the measured surfaces after first applying a tensile stress of 2400 psi (point A, where the axial plastic strain is approximately 0.11%), and subsequently following a path along which both axial and torsional loads varied, to point B (where the axial plastic strain is approximately 0.96%, and the plastic shear strain is approximately 1.4%). Even with these moderately small strains, the deviation from an idealized elliptical yield surface is clearly seen.

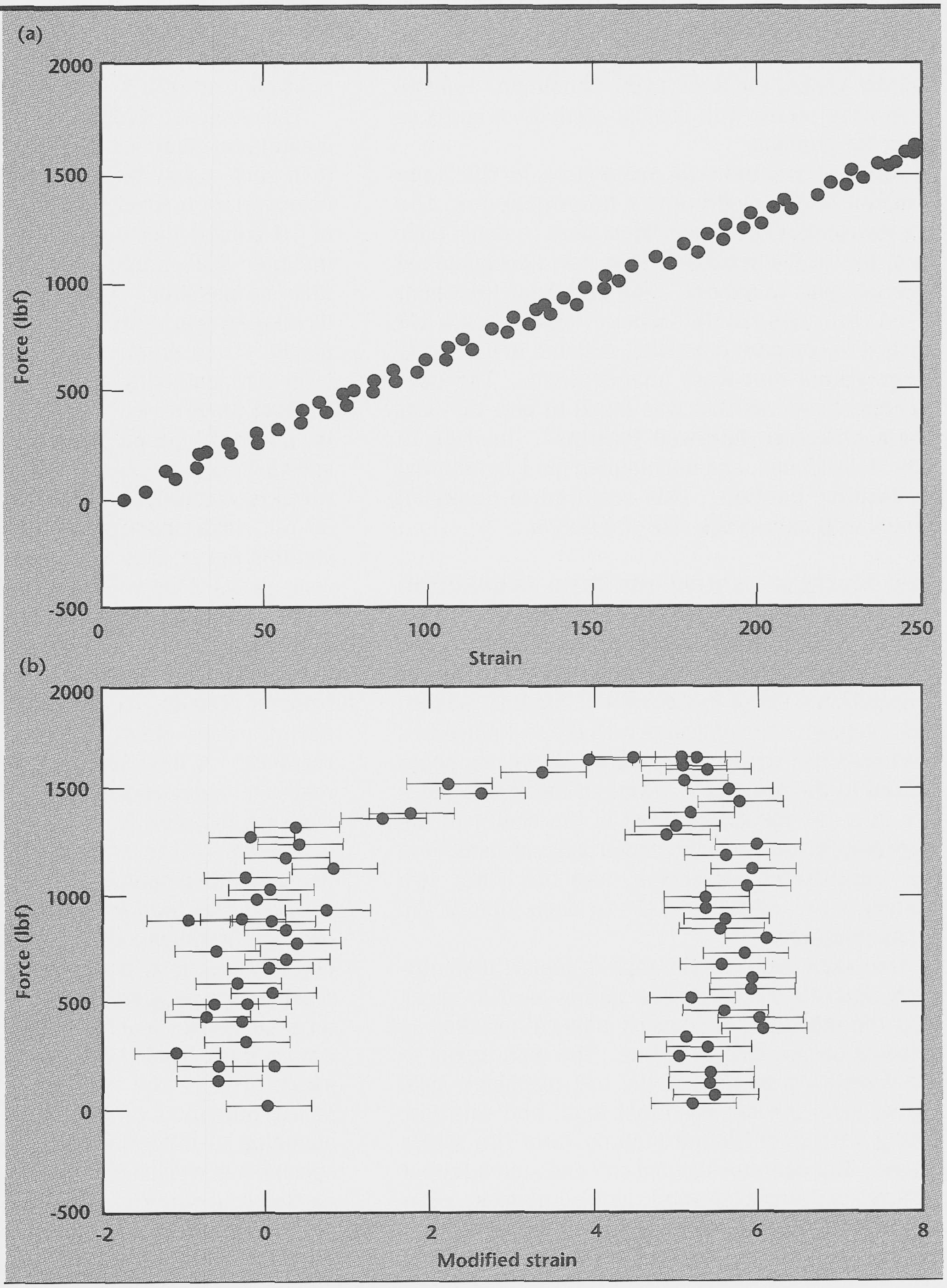

*Figure 2. A typical cross-plot of output data during loading and unloading, showing (a) load vs strain; and (b) load vs the modified strain measure described in the text. The yielding of the material is more readily seen in the load vs modified strain plot. The operator must simultaneously observe four such plots, corresponding to different strain-gage directions, to ensure detection of yield for an arbitrary direction of loading.*

## Future Work

We now have the ability to conduct novel experiments in finite plasticity. At present, the procedure requires significant operator expertise and interaction. Speed of testing could possibly be improved by automating the yield surface probing and mapping process via some control algorithm. However, this may not be a practical possibility in the near term, since the output data needs to be interpreted with a great deal of judgment during testing.

We plan to use these experiments to aid in the development of better constitutive equations for non-linear plasticity. We plan to examine materials of particular programmatic relevance, such as tantalum, which is a target material for the Multi-Scale Material Modeling effort. These experiments can be used to test predictions of models coming out of the multi-scale approach.

We also plan to conduct experiments to address an open question in the continuum theory of finite plasticity, namely the correct identification of the plastic strain tensor in the context of general finite deformations.[5,6]

## Acknowledgment

Contributions to this project from J. Casey result from work supported by a grant from the Solid Mechanics Program of the National Science Foundation, administered by the University of California, Berkeley. Part of the support for A. Brown's work, and material used during the development of the experimental procedure, were also provided through this grant.

## References

1. Naghdi, P. M. (1990), "Critical Review of the State of Finite Plasticity," *J. of Appl. Math. and Phys.* (ZAMP), **41**, pp. 315-394.

2. Groves, S., R. Sanchez, and W. Feng (1991), *Multiaxial Failure Characterization of Composites,* Lawrence Livermore National Laboratory, Livermore, CA, (UCRL-JC-105244).

3. Bell, J. (1983), "Continuum Plasticity at Finite Strain for Stress Paths of Arbitrary Composition and Direction," *Arch. Rat. Mech. Anal.,* **84**, pp. 201-232.

4. Phillips, A., C. Liu, and J. C. Justusson (1972), "An Experimental Investigation of Yield Surfaces at Elevated Temperatures," *Acta Mechanica,* **8**, pp. 119-146.

5. Casey, J., and P. M. Naghdi (1992), "A Prescription for the Identification of Finite Plastic Strain," *Int. J. Engr. Sci.,* **30**, pp. 1257-78.

6. Casey, J., and P. M. Naghdi, (1992), "On the Identification of Plastic Strain at Finite Deformation," *Defects and Anelasticity in the Characterization of Crystalline Solids,* L. M. Brock, Ed., ASME AMD Vol. **148**, pp. 11-33.

# Modeling of Shear Localization in Materials

**Donald R. Lesuer and Mary M. LeBlanc**
*Manufacturing and Materials Engineering Division*
*Mechanical Engineering*

**Robert A. Riddle and Bert R. Jorgensen**
*Defense Technologies Engineering Division*
*Mechanical Engineering*

The deformation response of a Ti alloy, Ti-6Al-4V, has been studied during shear localization. The study has involved well-controlled laboratory tests on a double-notch shear sample. The results have been used to provide a comparison between experiment and the predicted response using DYNA2D and two material models (the Johnson-Cook model and an isotropic elastic-plastic-hydrodynamic model). The work will serve as the basis for the development of a new material model that represents the different deformation mechanisms active during shear localization.

## Introduction

### Shear Localization

Shear localization is a common deformation and failure process that occurs when deformation is concentrated in a single macroscopic shear zone. It can occur in many materials at moderate and high strain rates due to localized, adiabatic heat production. Zener and Holoman[1] have estimated that during simple punching of a metal plate, the temperature increase in a shear band due to adiabatic heat production can be as high as 1000 °C. This increase in temperature produces thermal softening in the band and localization of plastic flow.

Shear localization is observed in many material processing operations, as well as during the in-service performance of materials. Typical material processing operations in which shear localization is observed include material cutting, numerous forming operations (such as rolling and forging), and material polishing.

In many cases, the success or failure of these processing operations is defined by shear localization. It is typically observed during the ballistic penetration and perforation of armor materials, the performance of munitions and explosive fragmentation, all problems of interest to programs at Lawrence Livermore National Laboratory (LLNL).

Despite its common occurrence and importance, shear localization remains poorly understood and is difficult to model accurately. Much of this difficulty arises from the large strains and adiabatic heat produced which, in turn, causes increases in temperature with resulting changes in material microstructure, material properties, and deformation mechanisms. Large changes in strain rate are also produced.

## Progress

Material models that can adequately represent the deformation response during shear localization must account for large strains (and the resulting strain hardening or softening), as well as large changes in strain rate and temperature. Several models have been developed that can represent, to varying degrees, the high rate deformation response of materials. Examples include models by Johnson-Cook (JC),[2] Zerilli-Armstrong (ZA),[3,4] and Follansbee-Kocks (mechanical threshold stress model)[5]. Two of these models (JC and ZA) have been introduced into the DYNA codes. Of these two models, the JC model is much more widely used, primarily because of the availability of material constants in the constitutive equations.

The objective of this project is to critically assess the ability of existing material models to represent the deformation response of materials during shear localization. We have done this using well-controlled laboratory experiments involving a double-notch shear sample. The experimental results have been compared with the predictions of the DYNA2D code using the JC model, as well as an isotropic elastic-plastic-hydrodynamic (EPH) model commonly used for large strain problems. The work will serve as the basis for the development of a new material model which represents the different deformation mechanisms active during shear localization.

## Material Models

The formulation for the JC model is empirically based, and represents the flow stress with an equation of the form,

$$\sigma = \left[A + B\varepsilon^{n}\right]\left[1 + C\ln\dot{\varepsilon}^{*}\right]\left[1 - T^{*}\right], \qquad (1)$$

where $\sigma$ is the effective stress; $\varepsilon$ is the effective plastic strain; $\dot{\varepsilon}^{*}$ is the normalized effective plastic strain rate (typically normalized to a strain rate of $1.0\ s^{-1}$); $T^{*}$ is the homologous temperature; n is the work hardening exponent; and A, B, C, and m are constants.

The values of A, B, C, n, and m are determined from an empirical fit of flow stress data (as a function of strain, strain rate, and temperature) to **Eq. 1**. For shear localization problems, we can assume that an arbitrary percentage of the plastic work done during deformation produces heat in the deforming material. For many materials, 100% of the plastic work becomes heat in the material. Thus, the temperature used in **Eq. 1** can be derived from the increase in temperature, according to the following expression:

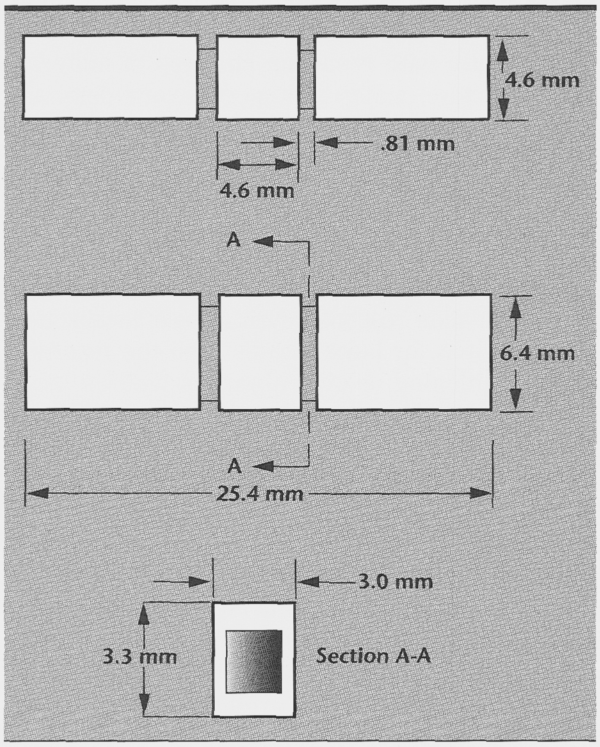

*Figure 1. Double-notch shear specimen used in this study.*

$$\Delta T = \frac{\alpha B}{\rho c\left(n+1\right)}\varepsilon^{n+1}, \qquad (2)$$

where $\Delta T$ is the temperature increase; $\alpha$ is the percentage of plastic work transformed to heat; c is the heat capacity; and $\rho$ is the density.

The EPH model uses an arbitrary effective stress/effective plastic strain curve, while a tensile cut-off pressure is defined for the principal stress spall criterion. A linear polynomial was chosen to define the hydrostatic equation of state. Material properties were derived from handbook data. The model is a popular choice for large strain plasticity problems. However, it does not account for strain rate or temperature effects and thus its accuracy for predicting deformation response during shear localization is largely unknown.

## Experiments

The double-notch shear sample, which is shown schematically in **Fig. 1**, is designed to produce a homogeneous strain state of pure shear in the gage section of the sample at a reasonably constant displacement velocity. Deformation in the gage section becomes localized and adiabatic shear can result. The samples were loaded using a split Hopkinson pressure bar (SHPB) apparatus and data was obtained at strain rates of $10^{-3}$ to $10^{-4}\ s^{-1}$. A schematic diagram of this apparatus is shown in **Fig. 2**.

In the SHPB tests, the strain histories for the incident ($\varepsilon_I(t)$) and transmitted ($\varepsilon_T(t)$) waves were measured and analyzed to determine the nominal shear stress/strain/strain-rate response of the sample during the shear test. The stress and strain-rate response were calculated from the following expressions:

$$\tau\left(t\right) = E\frac{A_0}{A}\varepsilon_T\left(t\right), \qquad (3)$$

and

$$\dot{\gamma}\left(t\right) = \frac{-2C_0}{L}\varepsilon_R\left(t\right), \qquad (4)$$

with

$$\varepsilon_I(t) + \varepsilon_R(t) = \varepsilon_T(t), \tag{5}$$

where $\tau(t)$ is the shear stress; E is the elastic modulus of the bar; $A_0$ is the cross-sectional area of the bar; A is the specimen shear area; $\dot{\gamma}(t)$ is the shear strain rate; $C_0$ is the longitudinal sound velocity in the bar; L is the gage length; and $\varepsilon_R(t)$ is the reflected strain in the bar. The resulting strain in the sample, $\varepsilon(t)$, was obtained by integrating the strain rate history:

$$\gamma(t) = \int_{t_0}^{t} \dot{\gamma} dt . \tag{6}$$

During FY-97, experiments and simulations of the double-notch shear experiment were done for a Ti alloy, Ti-6Al-4V. The tests were done at a number of different projectile velocities to get experimental results over a range of strain rates.

## Results and Analysis

**Modeling.** Simulations of the experiment were performed using the finite element code DYNA2D and the two material models described above, the isotropic EPH model (number 10) and the JC model. The simulations were used as an aid in both specimen and experiment design, as well as to evaluate the material models.

For the specimen design studies, three notch configurations were considered. Additional details of the simulations and the results are available in other references.[6,7]

Previous studies[8,9] using the double-notch shear specimen have shown that significant plastic bending can occur in the sample, which can cause deviations from the desired strain state of pure shear. The finite element simulations show that these bending effects can be minimized with proper specimen design. The results showed that a specimen containing a square notch (with corner radius equal to .002 in.) on all four sides of the sample had the highest ratio of shear strain to bending, and thus was selected for the experimental work.

The resulting specimen, shown in **Fig. 1**, is a significant improvement over test sample configurations used by other investigators. Simulations were also done to show the influence of important experimental variables, such as projectile length, incident bar length and strain gage placement. Results here were a significant aid in experiment design and data interpretation.

The deformed configuration for a sample tested with a projectile velocity of 1000 in./s is shown in **Fig. 3**. The specimen is near the point of maximum deformation and bending in the specimen is evident. Contours of effective plastic strain are also shown and illustrate that deformation is concentrated in an arc through the gage section. Similar deformation patterns and failure modes were obtained for both the JC and the EPH material models. Post-test examination of tested samples confirms the predictions of the simulations and shows that deformation was concentrated in an arc through the gage section. However, the JC model predicts greater deformation for a given projectile impact velocity. This is primarily a result of the softening caused by temperature increases in the shear zone.

**Experimental Results.** Experiments were conducted over a range in strain rates from an average shear strain rate of $3.8 \times 10^3$ to $1.1 \times 10^4$ s$^{-1}$. The shear stress and shear strain were calculated

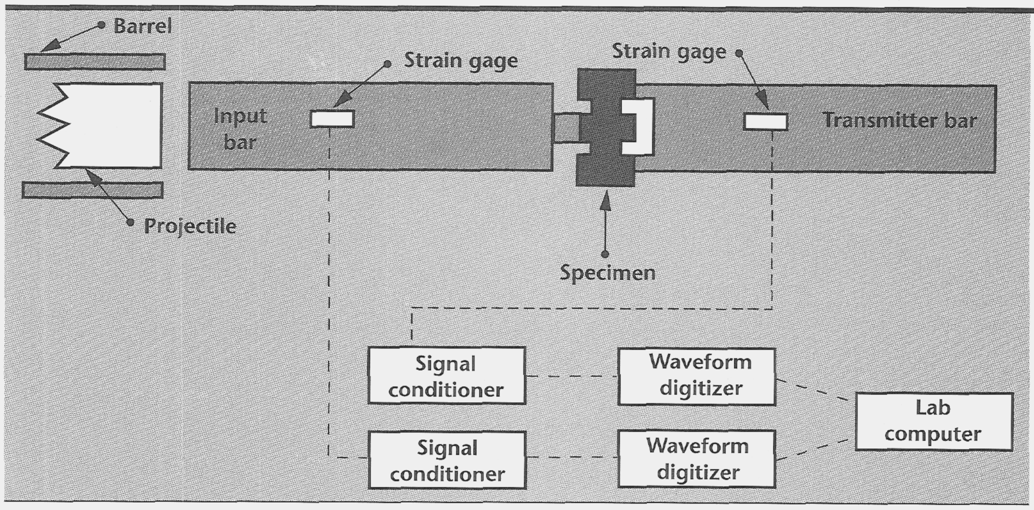

*Figure 2. Schematic diagram of the split Hopkinson pressure bar apparatus used to load the double-notch shear specimen.*

using **Eqs. 3, 4,** and **6**. The effective stress and effective plastic strain were then determined from the following expressions:

$$\sigma = \sqrt{3}\tau \tag{7}$$

and

$$\varepsilon_p = \left(\gamma - \tau/G\right)/\sqrt{3}\,, \tag{8}$$

where $\sigma$ is the effective stress; $\varepsilon_p$ is the effective plastic strain; and G is the shear modulus. The effective stress/effective plastic strain response of the sample is shown in **Fig. 4** for a test conducted at 7000 $s^{-1}$. The adiabatic temperature rise in the sample is also shown in the figure. Sufficient flow localization occurred to promote ductile fracture with a shear strain of about .25 (effective plastic strain of about .14). Despite the limited strains-to-failure, a temperature increase in the sample of about 40 °C is expected.

**Figure 5** shows a macro-photograph of a typical failed sample. Examination of samples deformed to strains near, but slightly less than, the failure strain showed cracks at the square corners of the gage section. The cracks resulted from the stress concentration at the corners and were the origins of failure. Final shear fracture occurred along an arc in the gage section due to intense plastic shear, which is consistent with the predictions of the finite element simulations shown in **Fig. 3**. The critical condition for shear fracture was obtained before significant thermal softening could be obtained.

The stress/strain response of the sample, as predicted by the simulation, was determined for an element in the center of the gage section. Calculations were done for both the EPH and the JC material models. The results are shown in **Fig. 4**, and compared against experimental data. The EPH model predicts flow stresses that are typically 200 to 300 MPa greater than those observed experimentally.

*Figure 3. Simulation results showing the deformed configuration and contours of effective plastic strain for the double-notch shear test. Sample was loaded with a projectile velocity of 1000 in./s.*

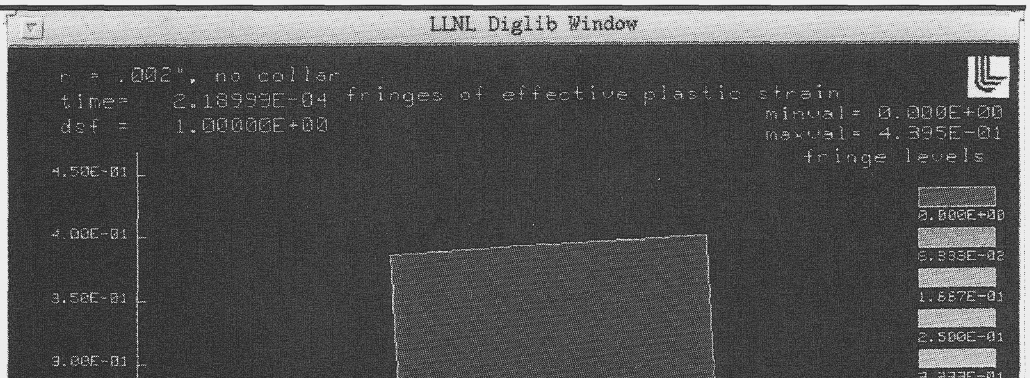
LLNL Diglib Window
r = .002", no collar
time= 2.18999E-04
dsf = 1.00000E+00
fringes of effective plastic strain
minval= 0.000E+00
maxval= 4.395E-01
fringe levels
0.000E+00
8.333E-02
1.667E-01
2.500E-01
3.333E-01
4.167E-01
5.000E-01
5.833E-01
6.667E-01
7.500E-01
8.333E-01
9.167E-01
4.50E-01
4.00E-01
3.50E-01
3.00E-01
2.50E-01
2.00E-01
1.50E-01
1.00E-01
5.00E-02
0.00E+00
-5.00E-02
-1.00E-01
-1.50E-01
-3.00E-01
-2.50E-01
-2.00E-01
-1.50E-01
-1.00E-01
-5.00E-02
0.00E+00
5.00E-02
1.00E-01
1.50E-01
2.00E-01
2.50E-01
3.00E-01

The calculations also predict a positive work hardening rate that is not observed experimentally. Some of these differences are due to the material model, which does not account for adiabatic heat, the resulting increase in temperature, and the decrease in strength. Experimental data available in the literature shows that the 40-°C increase in temperature observed here could lower the flow stress by about 100 MPa.[10] For the JC model, the predicted flow stress in the sample is about 100 MPa higher than that observed experimentally. Thus, the JC model shows closer agreement with experimental data than the EPH model. In addition, the JC model shows some thermal softening due to adiabatic heat production, which is consistent with experimental observations.

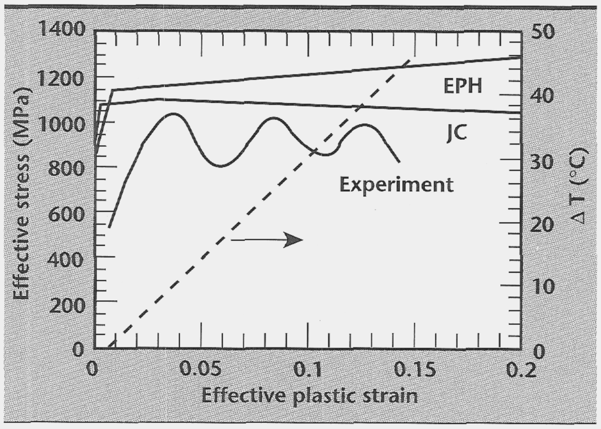

*Figure 4. Simulation results and experimental data of effective stress vs effective plastic strain for the double-notch shear sample shown in Figure 1. Results are shown for both the Johnson-Cook and the elastic-plastic-hydrodynamic material models. Adiabatic temperature increase is shown in the figure. Deformation rate is 7000 $s^{-1}$.*

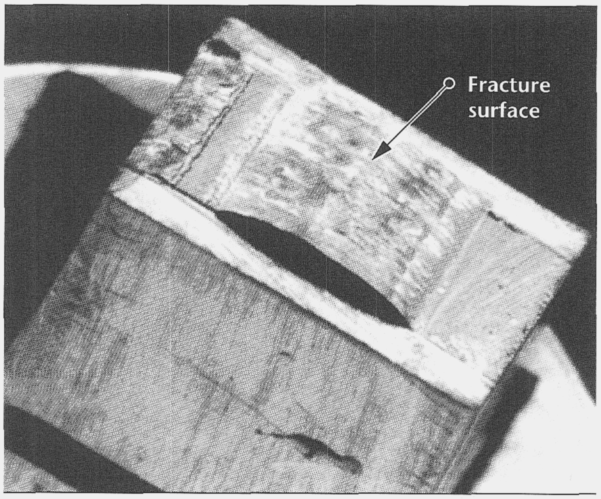

*Figure 5. Macro-photograph of a typical fractured sample. The fracture surface is indicated. Final fracture occurred along an arc in the gage section due to intense plastic shear.*

## Summary and Conclusions

The deformation response of a Ti alloy, Ti-6Al-4V, has been studied during shear localization. The study has involved well-controlled laboratory tests involving a double-notch shear sample. The results have been used to provide a comparison between experiment and the predicted response using DYNA2D and two material models. The primary conclusions from the study are as follows:

1) The deformation of the double-notch shear specimen has been studied using finite element analysis and an optimal specimen design for obtaining shear stress/shear strain data at high rates has been established.
2) The simulations show that deformation is concentrated in an arc through the gage section. Post-test examination of fractured samples shows that the simulations for both the EPH and the JC material models can represent the macroscopic deformation and fracture patterns observed in the sample.
3) For the Ti-6Al-4V alloy studied, shear fractures were obtained with a shear strain of about .25. A temperature increase of about 40 °C is expected.
4) The EPH model predicted flow stresses that were 200 to 300 MPa higher than experimental data. The calculations also predicted a positive work hardening rate that is not observed experimentally.
5) The JC model predicts flow stresses in the test sample that are closer to experimental data than the EPH model. In addition, the model correctly predicts the thermal softening observed experimentally.

## References

1. Zener, C., and J. H. Hollomon (1944), "Effect of Strain Rate Upon Plastic Flow of Steel," *Journal of Applied Physics,* January, **15**, pp. 22–32.

2. Johnson, G. R., and W. H. Cook (1983), "A Constitutive Model and Data for Metals Subjected to Large Strains, High Rates and High Temperatures," *Proceedings of the Seventh International Symposium on Ballistics,* The Hague, Netherlands, pp. 541–547.

3. Zerilli, F. J., and R. W. Armstrong (1992), "The Effect of Dislocation Drag on the Stress-Strain Behavior of FCC Metals," *Acta Metallurgica et Materialia,* **40**, p. 1803.

4. Zerilli, F. J., and R. W. Armstrong (1990), "Description of Tantalum Deformation Behavior by Dislocation Mechanics Based Constitutive Relations," *Journal of Applied Physics,* **68**, p. 1580.

5. Follansbee, P. S., and U. F. Kocks (1988), "A Constitutive Description of the Deformation of Copper Based on the Use of the Mechanical Threshold Stress as an Internal State Variable," *Acta Metallurgica,* **36**, p. 81.

6. Jorgensen, B. R. (1997), *Double-Notch Shear Test Analysis Using Johnson-Cook Material Properties,* Lawrence Livermore National Laboratory, Livermore, CA.

7. Jorgensen, B. R. (1997), *A Parametric Study of Double-Notch Shear Tests Using Finite Element Analysis,* Lawrence Livermore National Laboratory, Livermore, CA.

8. Harding, J. (1985), "Double-Notch Shear Testing and Punch Loading," *Metals Handbook—Mechanical Testing*, J. R. Newby, Ed., ASM International, Materials Park, Ohio, Vol. **8**, p. 228.

9. Harding, J., and J. Huddart (1979), "The Use of the Double-Notch Shear Test in Determining the Mechanical Properties of Uranium at Very High Rates of Strain," *Mechanical Properties at High Rates of Strain, 1979,* J. Harding, Ed., The Institute of Physics, London, United Kingdom.

10. Eylon, D., J. R. Newman, and J. K. Thorne (1990), "Properties and Selection: Nonferrous Alloys and Special-Purpose Materials," *ASM Handbook,* ASM International, Materials Park, Ohio, Vol. **2**, p. 638.

# Modeling of Casting Microstructures and Defects

**Arthur B. Shapiro**
*New Technologies Engineering Division*
*Mechanical Engineering*

**J. Del Eckels**
*New Technologies Engineering Division*
*Mechanical Engineering*

We have developed and implemented a micro-model for uranium that uses experimental results to estimate nucleation and growth kinetics.

## Introduction

Our interest in casting is linked to Department of Energy (DOE) efforts to reduce hazardous waste and scrap produced by metal component fabrication processes. Improved processes for manufacturing plutonium and uranium components, for example, can minimize scrap metal, contaminated waste, and possible radiation exposure, and reduce the cost of equipment and facilities.

Casting is an ancient art that has been a trial-and-error process for more than 4000 years. To predict the size, shape, and quality of a cast product, manufacturers typically cast full-size prototypes. If one part of the process is done incorrectly, the entire process is repeated until an acceptable product is achieved.

One way to reduce the time, cost, and waste associated with casting is to use computer modeling to predict not only the quality of a product on the macro-scale, such as distortion and part shape, but also on the micro-scale, such as grain defects. Modeling of solidification is becoming increasingly feasible with the advent of parallel computers.

There are essentially two approaches to solidification modeling. The first is that of macro-modeling, where heat transfer codes model latent heat release during solidification as a constant, based solely on the local temperature. This approach is useful in predicting large-scale distortion and final part shape. The second approach, micro-modeling, is more fundamental. The micro-models estimate the latent heat release during solidification using nucleation and grain growth kinetics. Micro-models give insight into cast grain morphology and show promise in the future to predict engineering properties such as tensile strength.

The micro-model solidification kinetics can be evaluated using first principles or experiments. This work describes an implementation of a micro-model for uranium that uses experimental results to estimate nucleation and growth kinetics.

## Progress

### Mathematical Formulation

The primary and most obvious phenomenon controlling casting is the transfer of heat from the cooling metal to the mold and surroundings. The present needs of many foundries are being satisfied by relatively simple heat conduction modeling that merely indicates regions of risk for shrinkage porosity. Using empirical information, foundry engineers successfully cast parts used in life-critical applications, such as jet engine turbine components.[1]

However, DOE's vision is to move from empiricism to science-based design.

Heat conduction analysis codes model latent heat release during solidification as a constant, based solely on the local temperature. The next step in solidification modeling is to make the latent heat a function of the solidification fraction, which depends on the nucleation rate and grain growth rate. **Equation 1** expresses an energy balance for a small volume of liquid, equating the change in internal energy to heat lost by convection to the environment plus generation of latent heat during phase change:

$$\rho c\frac{dT}{dt} = -h\frac{A}{V}\left(T - T_\infty\right) + \rho L\frac{dV_s}{dt} \qquad (1)$$

where $V_s$ is the evolution of solid.

**Equation 1** can be re-arranged to give the rate of change of temperature for the control volume:

$$\frac{dT}{dt} = -\frac{h}{\rho c}\frac{A}{V}\left(T - T_\infty\right) + \frac{L}{c}\frac{dV_s}{dt}. \qquad (2)$$

The first term on the right hand side of **Eq. 2** reflects the effect of casting geometry (the ratio of the surface area of the casting to its volume) on the extraction of sensible heat; the second term takes account of the continuing evolution of latent heat of fusion during solidification. It can be seen from this equation that during solidification, heating will occur if the second term on the right of **Eq. 2** becomes greater than the first one. This is known as recalescence, and is shown graphically in **Fig. 1**.

$V_S$ depends on the number of nucleation sites (N) and the grain growth rate (dR/dt), as shown in **Eq. 3:**

$$\frac{dV_S}{dt} = N4\pi R^2\frac{dR}{dt}\left(1 - V_S\right). \qquad (3)$$

Micro-models estimate $V_S$ during solidification using nucleation and growth kinetics. Several kinetic rate equations have been reported in the literature.[2] Two different models can be used for the nucleation law: continuous nucleation, or instantaneous nucleation. An example of a continuous nucleation rate law is shown in **Eq. 4:**

$$\frac{dN}{dt} = \beta(T_l - T)\frac{dT}{dt}. \qquad (4)$$

For an instantaneous nucleation model, the number of grains per unit volume, N, is determined by counting the number of grains in a micrograph of the casting.

An undercooling-dependent equation was used to estimate the growth rate **(Eq. 5):**

$$\frac{dR}{dt} = \mu(T_l - T)^2. \qquad (5)$$

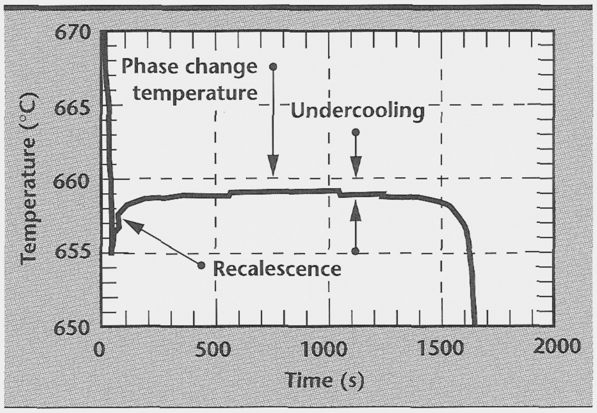

*Figure 1. Solidification curve. The curve is the temperature solution of Eqs. 2, 3 and 5, using the variables defined in Table 1. Notice the prediction of recalescence at 50 s.*

*Table 1. Symbols and values used in the solution of Eqs. 2, 3, and 5.*

| Symbol | Variable | Values |
|---|---|---|
| A | Area | $6.0 \times 10^{-4}$ m$^2$ |
| c | Heat capacity | 920 J/kg °C |
| h | Convection heat transfer coefficient | 2 W/m$^2$ °C |
| L | Latent heat | $4.44 \times 10^5$ J/kg |
| N | Number of nucleation sites | $1.0 \times 10^6$ grains/m$^3$ |
| R | Grain radius | |
| T | Temperature | |
| $T_\infty$ | Environment temperature | 25 °C |
| $T_l$ | Phase change temperature | 660 °C |
| t | Time | |
| V | Volume | $1.0 \times 10^{-6}$ m$^3$ |
| $V_S$ | Solid volume fraction | |
| $\beta$ | Nucleation rate law constant | |
| $\rho$ | Density | 2698 kg/m$^3$ |
| $\mu$ | Grain growth law constant | $3.0 \times 10^{-6}$ m/s (°C)$^2$ |

**Equations 2**, **3**, and **5** form a system of ordinary differential equations which can be solved numerically for the temperature, solid fraction, and grain radius, as a function of time. **Figure 1** shows the temperature response for a hypothetical material with properties defined in **Table 1**. Notice the phenomenon of recalescence occurring at a time of 50 s.

## Obtaining Rate Constants from Experimental Data

The evaluation of the kinetic laws based on first principles is in the formative stages. An alternate approach is to evaluate the rate constants from experimental results on a simple casting, and then apply the laws to a production casting model. This can be accomplished by recording temperature versus time data from a solidification experiment, and then using an optimization method to calculate the grain growth constant, $\mu$, by minimizing the difference between the experimental data and the temperature response calculated by **Eqs. 2**, **3**, and **5**.

We validated the experimental procedure using aluminum. The recorded temperature data for the top thermocouple in the sample is shown in **Fig. 2**.

A schematic of the experimental apparatus is shown in **Fig. 3**. The size of the crucible and insulation was designed by numerical modeling to produce axial solidification. Notice the horizontal shape of the calculated temperature contours at the bottom of the crucible where we are trying to produce axial solidification **(Fig. 4)**.

The initial condition for all materials in the model was set to 1673 K. Convection and radiation boundary conditions were specified on all exterior surfaces with a convection heat transfer coefficient of 5 W/m$^2$ °C, an ambient temperature of 298 K, and a surface emissivity of 0.8.

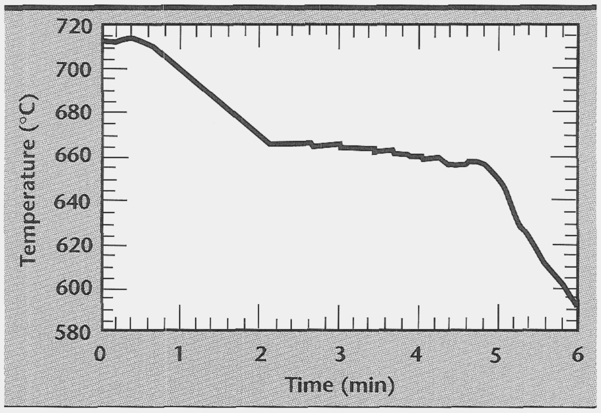

*Figure 2. Temperature history recorded by the top thermocouple in Figure 3, for aluminum solidification in the crucible.*

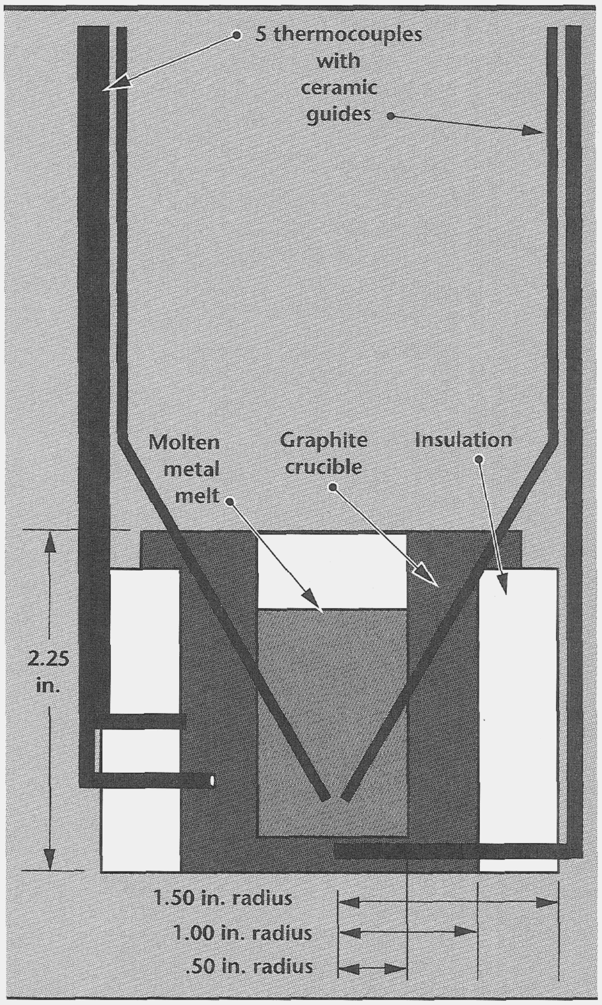

*Figure 3. Schematic of the experimental apparatus. The apparatus was designed using numerical modeling to produce 1-D axial solidification, shown in Figure 4.*

## Future Work

We have developed a methodology to calculate solidification kinetic rate constants and have validated the experimental procedure using aluminum. Future plans are to conduct the experiment using uranium. We plan to calculate the rate constants using the Global Local Optimization code.[3]

*Figure 4. Calculated temperature (K) contours during solidification. Notice the horizontal shape of the contours at the bottom of the crucible where we are trying to produce axial solidification between the two thermocouple positions, as indicated in Figure 3.*

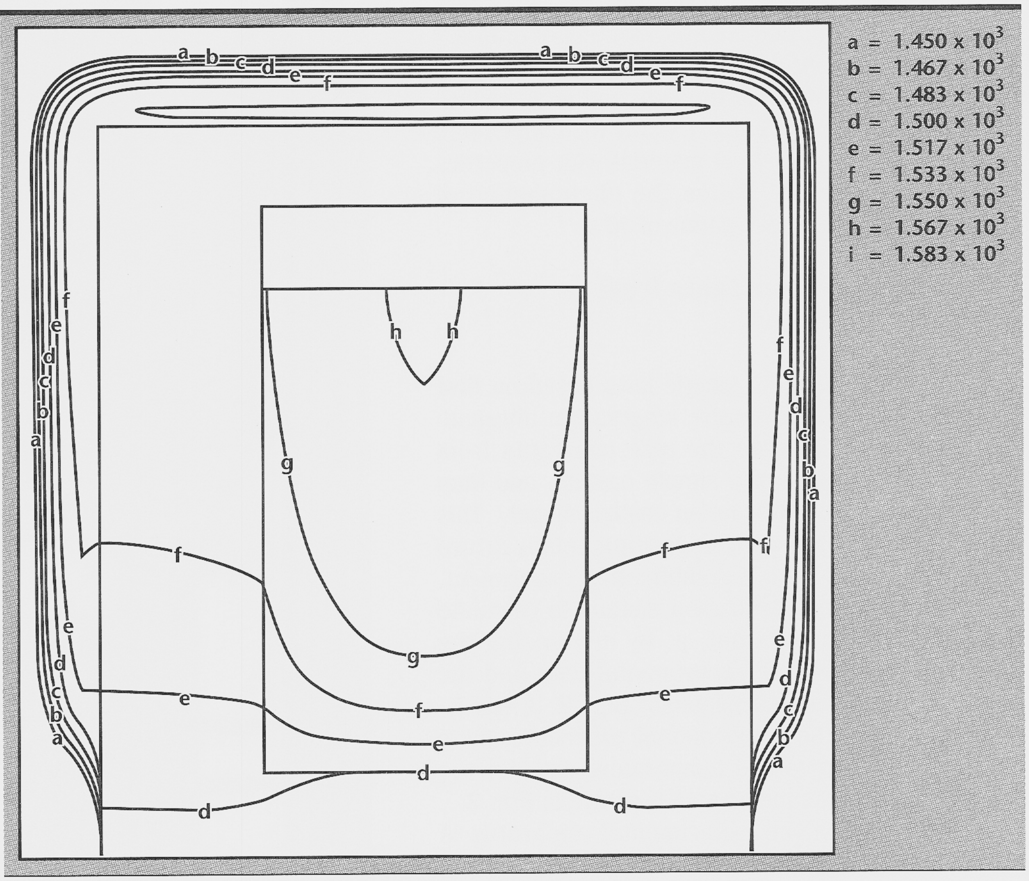

## References

1. Tu, J. S., and R. K. Foran (1992), “The Application of Defect Maps in the Process Modeling of Single Crystal Investment Casting,” *Journal of Metals*, June, pp. 26–28.

2. Stefanescu, D. M., G. Upadhya, D. Bandyopadhyay, and I. G. Chen (1989), “Modeling the Evolution of Equiaxed Microstructure in Castings,” *Journal of Metals*, February, pp. 22-25.

3. Murphy, M. J. (1996), *GLO User's Manual*, University of California, Lawrence Livermore National Laboratory, Livermore, CA.

Technical Information Department
Lawrence Livermore National Laboratory
University of California
Livermore, California 94551